Volume 22, No 3 | International Journal of Radiation Research, July 2024

# Fluoro-2-deoxy-D-glucose ($^{18}$F-FDG) positron slowing down, annihilation, and electron capture absorbed doses in female patients

**F. Mohajeri[1], A. Ezzati[1*], M. Studenski[2]**

*[1]The University of Tabriz, Department of Physics, Tabriz, Iran*
*[2]The University of Miami, Department of Radiation Oncology, 33136, Miami, FL, USA*

► ***Original article***

***Corresponding author:***
*Dr. Ahad Ollah Ezzati,*
***E-mail:***
*ah_ezzati63@yahoo.com*

**Received:** July 2023
**Final revised:** December 2023
**Accepted:** January 2024

***Int. J. Radiat. Res., July 2024; 22(3): 559-564***

**DOI:** 10.61186/ijrr.22.3.559

***Keywords:*** *PET imaging, Radiation dosimetry, Monte Carlo, Uptake biokinetics, $^{18}$F-FDG.*

## ABSTRACT

***Background***: 18-F fluoro-2-deoxy-D-glucose ($^{18}$F-FDG) is the most common tracer in whole-body positron emission tomography (PET) imaging for cancer. The diagnostic information gained from a 18F-FDG is beneficial, but the administration of radioactive material always comes with an increased risk of secondary cancer. The objective of this paper was to calculate the effective dose for $^{18}$F-FDG injected patients considering the specific contribution from positron slowing down, positron annihilation, and electron capture mechanisms. ***Materials and Methods:*** The dose for various organs was estimated by using the Monte Carlo (MC) method. The Medical Internal Radiation Dose (MIRD) female phantom was used for the simulations and the effective doses to various organs from internal exposure from a $^{18}$F-FDG injection were calculated using a biokinetic model and International Commission on Radiological Protection (ICRP) publication 128 provided data. Calculated doses were compared with measured doses found in published studies. ***Results:*** The dose for each organ is dependent on the $^{18}$F decay mode. The total effective dose is 6.73 mSv when the administered activity is 185 MBq. Positron annihilation leads to the highest average effective dose at 3.57 mSv. The effective doses for positron slowing and electron capture gammas are 2.99 and 0.17 mSv, respectively. The urinary bladder, followed by the brain and heart, have the highest absorbed doses. The calculated doses for a female patient are in good agreement with published measured data. ***Conclusions:*** The results presented here can be used to scale the dose measured by a dosimeter to estimate the patient's absorbed dose. Tracking the cumulative effective dose from medical procedures is an important aspect of managing the care of cancer patients to ensure regulatory limits are not exceeded.

## INTRODUCTION

Positron emission tomography (PET) has become an important imaging modality globally for many patients. The major advantage of PET imaging is the non-invasive quantification of biochemical and functional processes rather than simple anatomical imaging [(1)]. The most common tracer used in PET imaging is 18-F fluoro-2-deoxy-D-glucose ($^{18}$F-FDG). $^{18}$F-FDG PET is a sensitive medical imaging modality that can be used for the detection, staging, re-staging, and therapy response evaluation in treating various cancers [(1-3)].

PET scanners are typically merged with a computed tomography (CT) scanner and the resulting PET/CT has the advantage of providing both anatomical and functional information. The downside is the increased radiation dose when compared to other imaging modalities, since patients are exposed both internally and externally [(2-4)]. Patient doses must be monitored, especially with repeat scanning, to balance the benefits of radiation exposure risk versus the diagnostic information gained. Periodic dose monitoring is critical as it allows the nuclear imaging staff to track the patient and alert if the cumulative radiation dose exceeds action levels [(5)]. Unfortunately, the current data on the radiation doses, especially the effective dose to oncology patients who received PET imaging, is limited. One major issue is the uncertainty in dose calculation from internally administered radiotracers. Without more exact dosimetry, the only means of limiting radiation dose is by following the appropriate use criteria (AUC) [(6)].

Measuring internal radiation dose is difficult as dosimeters cannot be placed into the various organs without surgical complications. Simulation techniques such as the Monte Carlo (MC) method, allow for dose calculation by tracking millions of particles as they traverse the patient and deposit dose. Monte Carlo N-particle transport (MCNP, Los Alamos National Laboratory, USA) [(6)] is a multi-purpose radiation particle transport code for modeling the radiation interaction with matter,

[ Downloaded from mail.ijrr.com on 2025-10-14 ]

[ DOI: 10.61186/ijrr.22.3.559 ]

including powerful three-dimensional geometry and source modeling capabilities that could be used in medical physics and nuclear medicine [7]. Recently, papers have reviewed the principles of using MC simulations in single photon emission computed tomography (SPECT) and PET imaging systems [6, 8, 11]. In this work, we will focus on MC simulation of PET to estimate the effective dose for a patient based on the different mechanisms found in the positron decay process. An adult female Medical Internal Radiation Dose (MIRD) phantom was used to measure absorbed dose in selected organs. In addition, the absorbed doses for positron slowing down, positron annihilation, and electron capture were calculated for different organs providing a comprehensive approach to calculating the effective dose for whole-body PET imaging. This study provides valuable insights into the potential risks and safety considerations associated with this imaging technique for female patients, contributing to improved patient safety and dosimetry in nuclear medicine.

The results of this study will provide important scaling factors that can be used to improve the accuracy of dosimetry for patients undergoing PET imaging procedures. Accurate dosimetry is essential for ensuring the safety and effectiveness of these procedures for patients, especially cancer patients who receive multiple imaging examinations. By obtaining more precise scaling factors, healthcare providers can assess the appropriate imaging studies to maximize the therapeutic benefit while reducing the potential risk of secondary cancer from radiation exposure.

## MATERIALS AND METHODS

### *Biokinetic modeling*

The female MIRD phantom (figure 1) was used in this study to simulate the human body and the various organs (Oak Ridge National Laboratory, USA) [12]. The details regarding the dimensions and composition of the phantom can be found in the literature [12, 13].

The simulated $^{18}$F-FDG activity was determined from the European Association of Nuclear Medicine/ Society of Nuclear Medicine and Molecular Imaging protocol (EANM/SNMMI), version 2.0 [16,17]. There is a relationship between the administered activity of $^{18}$F-FDG, weight, and duration of emission acquisition [14]. For the 78.65 kg simulated in this work, the minimum and maximum activities are 185 MBq and 462.3 MBq, respectively [14].

The $^{18}$F-FDG distribution was calculated according to the biokinetic equations accounting for both physical and biological half-lives inside the human body (table 1) [18]. Following intravenous administration of a radiotracer, most of the compound is cleared rapidly from the blood circulation where it accumulates within the larger organs. From there, it decays with the physical and biological half-lives described in table 1 [18]. It is assumed that all activity is excreted through the urinary system and that retention in the specific source organs is infinite (without consideration of a delayed uptake).

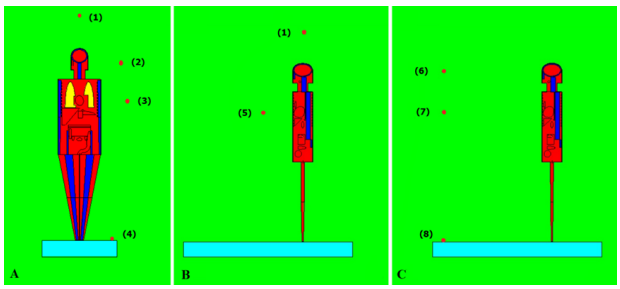


**Figure 1.** Female MIRD phantom showing the locations of the TLD in both the measurements and simulations **a)** In the XZ plane, the TLDs were positioned as follows: (1) 0.3 m superior to the head, (2) 0.3 m lateral to the head, (3) 0.3 m lateral to the chest, and (4) 0.3 m lateral to the feet. **b)** in the YZ plane, the TLDs were situated as follows: (5) 0.3 m anterior to the chest **c)** in the YZ plane, the TLDs were placed at (6) 1 m anterior to the head, (7) 1 m anterior to the chest, and (8) 1 m anterior to the feet.

**Table 1.** The biokinetic data for $^{18}$F-FDG [16].

| Organ | $F_s$ | $T_i$ (h) | $T_{i,\,eff}$ | $a_i$ | $\tilde{A}_s/A_0$(h) | $\tilde{A}_s/A_0$(h) [This study] |
|---|---|---|---|---|---|---|
| Brain | 0.08 | - | 1.83 | 1.0 | 0.21 | 0.211 |
| Heart wall | 0.04 | - | 1.83 | 1.0 | 0.11 | 0.105 |
| Lungs | 0.03 | - | 1.83 | 1.0 | 0.079 | 0.0792 |
| Liver | 0.05 | - | 1.83 | 1.0 | 0.13 | 0.132 |
| Urinary bladder contents | 0.24 | 0.2 | | 0.25 | 0.26 | 0.255 |
| | - | 1.5 | | 0.75 | - | - |
| Other organs and tissues | 0.80 | 0.2 | 0.18 | 0.075 | 1.7 | 1.707 |
| | - | 1.5 | 0.82 | 0.225 | - | - |
| | - | - | 1.83 | 0.70 | - | - |
| Total | - | - | - | - | 2.489 | 2.4892 |

*Abbreviations: $F_s$: fractional distribution of $^{18}$F-FDG to source organ or tissue S, $T_i$: biological half-life , $T_i$, eff: effective half-life for elimination component i, $a_i$: fraction of $F_s$ eliminated with a biological half-life $T_i$, $\tilde{A}_s/A_0$: accumulated activity in the organ or tissue S per unit of administered activity.

### *$^{18}$F-FDG source:*

MCNPX v2.7 was used to simulate a continuous positron spectrum with a maximum range of 2.4 mm and maximum energy of 0.64 MeV [15]. The $^{18}$F positron energy distribution was obtained via equations (1) and (2).

$$N(E) = C\sqrt{(E^2 + 2Em_ec^2)}\,(Q-E)^2(E+m_ec^2) \quad (1)$$

$$C = \frac{1}{\int_0^Q \sqrt{(E^2+2Em_ec^2)}\,(Q-E)^2(E+m_ec^2)} \quad (2)$$

In equations (1) and (2), $m_ec^2$ is the electron rest mass, E is the kinetic energy of the positron, Q is the maximum energy of the positron and $N$ is the relative

[ Downloaded from mail.ijrr.com on 2025-10-14 ]

[ DOI: 10.61186/ijrr.22.3.559 ]

number of the emitted positrons.

To perform radiation decay analysis calculations, we considered two particles: the 1.6559 MeV electron capture photon (with 0.0314 probability) and the positron emission (with 0.9686 probability). The activity was calculated using the biokinetic model with $1\times10^9$ histories. Each organ in the MIRD phantom was considered as a single compartment and the energy deposited in MeV (E) was calculated using a type 8 tally. The cumulated activity of the whole body (Ã) was calculated by integrating the individual organ activity ($A_i(t)$) over all time (equation 3).

$$\tilde{A} = \int_0^{\infty} \sum_i A_i(t)\, dt \qquad (3)$$

***Dose Calculation:***

Equation (4) was used to convert the deposited energy in each organ to dose.

$$D_{Total} = \tilde{A}\, E(MeV) \times \frac{1}{m}\left(\frac{1}{Kg}\right) \times 1\cdot6 \times 10^{-13} \frac{J}{MeV} = \tilde{A}\, E/m \times 1.6 \times 10^{-13} Gy \qquad (4)$$

In equation (4), m is the mass of the organ and E deposited energy per decay. To calculate the absorbed dose due to each specific decay mechanism, the input file was written to include only the emitted particle as a source. This allowed the calculation of the energy deposition in each organ due to electron capture ($E_{EC}$), positron annihilation ($E_{PA}$) and positron slowing down ($E_{PS}$). We used an electron spectrum with the same energy distribution as the positron to obtain $E_{PS}$. $E_{PA}$ was calculated by subtracting the $E_{PS}$ from the energy deposited in the organ due to position emission. The absorbed dose was then calculated using equations (5-7).

$$D_{EC} = \tilde{A}\ E_{EC}(MeV) \times \frac{1}{m}\left(\frac{1}{Kg}\right) \times 1\cdot6 \times 10^{-13} \frac{J}{MeV} \times 0.0314 = \tilde{A}\, E_{EC}/m \times 1.6 \times 10^{-13} \times 0.0314 Gy \qquad (5)$$

$$D_{PS} = \tilde{A}\ E_{PS}(MeV) \times \frac{1}{m}\left(\frac{1}{Kg}\right) \times 1\cdot6 \times 10^{-13} \frac{J}{MeV} \times 0.9686 = \tilde{A}\ E_{PS}/m \times 1.6 \times 10^{-13} \times 0.9686 \mathbf{Gy} \qquad (6)$$

$$D_{PA} = \tilde{A}\, E_{PA}(MeV) \times \frac{1}{m}\left(\frac{1}{Kg}\right) \times 1\cdot6 \times 10^{-13} \frac{J}{MeV} \times 0.9686 = \tilde{A}\, E_{PA}/m \times 1.6 \times 10^{-13} \times 0.9686 Gy \qquad (7)$$

***Effective Dose***

In addition to calculating the effecvtive dose to the organs noted in table 1, we found a high level of accumulation in bone. The bone model in the MIRD phantom does not differentiate between red and yellow marrow so we scaled the doses by the percentage of each component [16]. The whole-body effective dose was determined using Equation (8):

$$H_E = \sum_T W_T H_T \qquad (8)$$

where $W_T$ is the organ or tissue weighting factor based on ICRP 128 recommendations, and $H_T$ is the equivalent tissue dose [16].

***Simulation validation***

To validate our simulations, the measurement setups of Quinn *et al.* [17] were replicated in MCNPX. Eight thermo luminescent dosimeters (TLDs) were simulated around the patient after 77 min of tracer injection. As shown in figure 1, absorbed doses were calculated at three locations around the head (0.3 m superior/0.3 m lateral/1 m anterior), chest (0.3 m anterior/0.3 m lateral/1 m anterior) and feet (0.3 m lateral/1 m anterior). We simulated administered activities of 300 and 490 MBq to match the method from [17]. We used biokinetic model based activity distribution to determine the dose rate at 1 m from the chest anterior at 60 min post-injection (μSv/MBq.h) for normalization purposes [17].

We ran $8\times10^8$ histories using the same source distribution in the MIRD phantom as described above. The energy deposited (E) in each TLD was calculated using type 8 tallies. The energy deposited was converted to dose via equation (9):

$$D_{TLD}\ (Sv) = \tilde{A}(t) \times E(MeV) \times \frac{1}{m}\left(\frac{1}{Kg}\right) \times 1\cdot6 \times 10^{-13} \frac{J}{MeV} \qquad (9)$$

The accumulated activity *Ã(t)* after injection was calculated using equation (10) [18]:

$$\tilde{A}(t) = \int_0^t \sum_i A_i(u)\, du \qquad (10)$$

*A(u)* represents the activity in the source organ at time *u* while *t* is the time post-injection of $^{18}$F-FDG (4620 seconds):

To convert $D_{TLD}$ to unit *μSv/h*, equation (11) was used:

$$D_{EFF} = D_{TLD} \times 10^6/1.2895\ h \qquad (11)$$

The effective dose rate, represented by $D_{TLD}$, refers to the absorbed dose of the patient within a specific timeframe. It considers factors such as the type and energy of the radiation, as well as the varying sensitivity of organs and tissues to radiation.

## RESULTS

Figure 2 shows the $^{18}$F-FDG source distribution in the MIRD female phantom. Table 2 shows the organs and tissues absorbed doses of the patient after injection of 185 MBq $^{18}$F-FDG. Also, the contribution of each decay particle of $^{18}$F is expressed. The effective dose of positron annihilation is 3.57 mSv, which is higher than the other modes. Also, 2.99 mSv is associated with the positron slowing down dose and 0.17 mSv to the electron capture gammas. These results agree with the total effective dose calculations. The highest absorbed dose of electron capture, positron annihilation, and positron slowing

[ Downloaded from mail.ijrr.com on 2025-10-14 ]

[ DOI: 10.61186/ijrr.22.3.559 ]

down was observed in the urinary bladder, followed by the brain and heart. The urinary bladder's absorbed dose by positron slowing down is approximately 2.27-fold higher than those for the positron annihilation. The brain has the next highest dose for all emitted particles, which are 1.26E-04, 2.76E-03, and 3.44E-03 Gy, for electron capture, positron annihilation, positron slowing down, respectively. The absorbed dose of the heart by different decay modes are 1.27E-04, 2.77E-03, and 3.35E-03 Gy for electron capture, positron annihilation and positron slowing down, respectively. The adrenal and arm bone has the lowest absorbed dose. The lung's absorbed dose is higher in positron slowing down, but the uterus absorbed dose is higher for other modes. The absorbed dose from positron decay in the lungs was approximately 1.4-fold higher than the absorbed dose from positron annihilation. The total effective dose was calculated as 6.73 mSv, using the female reference phantoms combined with the tissue-specific weighting factors relative to ICRP 128.

The normalized dose rate at 1 m from the chest anterior, 60 min post-injection was found to be 0.063 μSv/MBq h. This value is in good agreement with the effective dose rate value measured by Quinn *et al.* [20] which was 0.067±0.022 μSv/MBq h. table 3 displays the calculated dose rates for Quinn *et al.* [20] measurement setups, including the measured dose rates for comparison. The simulations conducted in this study and measurements taken by Quinn *et al.* are in good agreement.

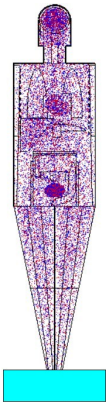

**Figure 2.** The distribution of 18F -FDG source in a female MIRD phantom, plotted using VISED. The red points represent electrons, while the blue points represent photons.

**Table 2.** The absorbed dose (in Gy) and effective dose (in mSv) of all organs in the patient after the injection of 185MBq $^{18}$F-FDG.

| Organs | Electron capture dose (Gy) | Positron annihilation dose (Gy) | Positron slowing down dose (Gy) | Total absorbed dose (Gy) |
|---|---|---|---|---|
| trunk | 6.20E-05 | 1.28E-03 | 5.43E-04 | 1.88E-03 |
| head | 3.04E-05 | 6.31E-04 | 5.36E-04 | 1.19E-03 |
| adrenals | 2.71E-05 | 2.63E-05 | 2.65E-04 | 8.64E-04 |
| uterus | 1.14E-04 | 2.43E-03 | 5.37E-04 | 3.10E-03 |
| thymus | 5.99E-05 | 1.23E-03 | 5.55E-04 | 1.92E-03 |
| spleen | 5.08E-05 | 1.04E-03 | 5.40E-04 | 1.63E-03 |
| pancreas | 6.49E-05 | 1.38E-03 | 5.38E-04 | 1.95E-03 |
| kidney | 5.32E-05 | 1.09E-03 | 5.38E-04 | 1.65E-03 |
| heart | 1.27E-04 | 2.77E-03 | 3.35E-03 | 6.26E-03 |
| gall bladder | 7.06E-05 | 1.49E-03 | 5.39E-04 | 2.06E-03 |
| stomach | 5.61E-05 | 1.15E-03 | 5.38E-04 | 1.75E-03 |
| lung | 6.05E-05 | 1.31E-03 | 1.84E-03 | 3.22E-03 |
| large intestine, colon | 6.87E-05 | 1.44E-03 | 5.37E-04 | 2.05E-03 |
| small intestine | 6.53E-05 | 1.37E-03 | 5.41E-04 | 1.98E-03 |
| breasts | 4.31E-05 | 8.47E-04 | 5.32E-04 | 1.42E-03 |
| ovaries | 7.37E-05 | 1.71E-03 | 5.58E-04 | 2.43E-03 |
| urinary bladder & contents | 4.56E-04 | 1.03E-02 | 2.34E-02 | 3.41E-02 |
| esophagus | 6.98E-05 | 1.49E-03 | 5.55E-04 | 2.14E-03 |
| liver | 8.52E-05 | 1.82E-03 | 1.60E-03 | 3.50E-03 |
| thyroid | 5.39E-05 | 1.10E-03 | 5.38E-04 | 1.60E-03 |
| skin | 2.53E-05 | 5.20E-04 | 5.32E-04 | 1.08E-03 |
| brain | 1.26E-04 | 2.76E-03 | 3.44E-03 | 6.31E-03 |
| salivary glands | 6.85E-05 | 1.44E-03 | 5.53E-04 | 2.09E-03 |
| arm bones up | 4.14E-05 | 8.24E-04 | 4.06E-04 | 1.28E-03 |
| arm bones down | 2.42E-05 | 4.79E-04 | 4.00E-04 | 9.01E-04 |
| spine | 5.60E-05 | 1.21E-03 | 4.04E-04 | 1.67E-03 |
| cranium, facial skeleton | 6.54E-05 | 1.40E-03 | 4.26E-04 | 1.87E-03 |
| pelvis | 5.65E-05 | 1.23E-03 | 4.02E-04 | 1.69E-03 |
| legs up | 3.82E-05 | 7.78E-04 | 5.37E-04 | 1.36E-03 |
| legs down | 2.18E-05 | 4.48E-04 | 5.36E-04 | 1.01E-03 |
| rib cage, clavicles, scapulae | 4.05E-05 | 8.37E-04 | 4.04E-04 | 1.28E-03 |
| leg bones up | 5.08E-05 | 1.08E-03 | 4.03E-04 | 1.53E-03 |
| leg bones down | 3.73E-05 | 7.78E-04 | 4.06E-04 | 1.21E-03 |
| Effective dose (mSv) | 0.17 | 3.57 | 2.99 | 6.73 |

**Table 3.** The effective dose rates (μSv/h) calculated and measured during a 77-minute period after the injection of $^{18}$F-FDG. The measurements were taken at various distances from the head, chest, and feet of the patient.

| | | Dose rate (μSv h$^{-1}$) | | | | | | | |
|---|---|---|---|---|---|---|---|---|---|
| | | Measurement [17] (Min-Max) | | | | Simulation | | | |
| | Activity (MBq) | 0.3 m sup | 0.3 m lat | 0.3 m ant | 1 m ant | 0.3 m up | 0.3 m lat | 0.3 m ant | 1 m ant |
| Head | 490 | (40–80) | (62–108) | - | - | 59.92 | 60.92 | - | - |
| | 300 | - | - | - | (7–22) | - | - | - | 14.52 |
| Chest | 490 | - | (48–120) | (69–151) | - | - | 76.50 | 128.15 | - |
| | 300 | - | - | - | (10–26) | - | - | - | 16.61 |
| Feet | 490 | - | (12.1–21.9) | - | - | - | 25.33 | - | - |
| | 300 | - | - | - | (5–16) | - | - | - | 11.15 |

*Abbreviations: sup: superior, lat: lateral, ant: anterior.

[ Downloaded from mail.ijrr.com on 2025-10-14 ]

[ DOI: 10.61186/ijrr.22.3.559 ]

## DISCUSSION

With improved treatment techniques, cancer patients have increased survival necessitating repeat oncologic imaging such as PET. It is essential to have a comprehensive understanding and consideration of the variability and uncertainty in dose estimation for these studies so the cumulative dose can be tracked over time. Numerous factors contribute to the uncertainty in calculating the absorbed dose of organs. These factors include energy deposition through MC calculation, distribution and biokinetics of radiopharmaceuticals at the organ level, variations in body morphometry between the patient and the phantom representing the patient, tumor type and location, and uncertainties in the physical decay data of radionuclides [19,22].

The current literature on PET dosimetry focuses on total effective dose, not on the specific components. The total effective dose encompasses the cumulative impact of radiation exposure on the body's organs, while specific components of radiation refer to the affected organ or tissue. Our research is centered on examining the effects of radiation on both individual organs and the body as a whole. In fact, our study specifically looks at the overall impact of radiation on the entire body, providing a comprehensive and specific view of radiation exposure in PET imaging. Khamwan *et al*. determined the effective dose for 35 oncology Thai patients with the age range of 28–60 y from PET/CT scan using $^{18}$F-FDG. The average whole-body effective doses were 4.40+0.61 and 14.45+2.82 mSv, for PET and CT respectively. They reported that the total patient dose was 18.85 mSv which could be used as the reference dose in Thai patients [23] Said *et al*. estimated the total effective dose of $^{18}$F-FDG examination as a function of the mean value of the patient's weight, height, and patient body mass index (BMI). A total of 82 oncology patients (44 males and 38 females) were considered. The total effective dose of $^{18}$F-FDG PET/CT for male patients was 20.2 ± 8.6 mSv and for female patients was 19.0 ± 8.2 mSv. The mean values of weight, height and interval were 66.9 ± 17.5 kg, 160.1 ± 18.4 cm, and 29.7 ± 4.9 kg/m2, respectively. In PET dosimetry, when the patient's administered activity was 424.8 ± 125.9 (205.7 – 675.9) MBq, PET effective dose is 8.1 ± 2.4 (3.9 – 12.8) mSv [2]. In another studies [2, 24], patients with weights between 31-50 kg and 50-70 kg were selected for dose estimation and PET effective doses were within the range of 5 mSv and 6-10 mSv. Patients with weight more than 70 kg receive effective doses within 11-15 mSv. By increasing the patient's weight, his/her absorbed dose increased because the administered activity of $^{18}$F-FDG was set to 5 MBq/kg of the patient's body weight. While our overall results are comparable to these studies, our work delves deeper into the specific components of PET dosimetry. We provide detailed calculations for organ and tissue doses, emphasizing the significance of considering individual patient characteristics.

Additionally, we found that the effective dose of the oncology patients who undergo whole body $^{18}$F-FDG PET/CT imaging was 11.5 ± 5.0 mSv, which was less than the previously reported values ranging from 21.46 to 25 mSv. Thus, the patients' weight is a crucial factor in PET dosimetry for $^{18}$F-FDG [25]. In our study, we observed that a female patient who received an injection of 185 MBq of 18F-FDG was exposed to a total effective dose of 6.73 mSv during PET imaging. This value falls within the range of 6.5 to 16.5, as reported by Kaushik *et al*. which confirms the accuracy of our results. It has been proven that the effective absorbed doses for PET/CT procedures have variations ranging from 8.0 to 80.0 mSv, when 370 MBq of $^{18}$F-FDG was administered [26]. Also, the effective dose in each method, calculated the use of Organ Level Internal Dose assessment (OLINDA) software, was up to 17.7% higher than the effective dose estimation using IDAC2.1 software (0.016 mSv/ MBq effective dose per administered activity for $^{18}$F-FDG) [27,28]. The variation in patient effective dose is nearly certainly because of variation in the administered activity, based on patient mass, an estimate of post-injection waiting time, and type of pathology [2]. We used the MCNP code to determine the effective dose per administered activity for $^{18}$F-FDG (0.036 mSv/MBq) which is up to 55.6% higher than the effective dose estimate obtained from IDAC2.1 software. This finding is in line with results from experimental studies.

## CONCLUSION

In this study, we calculated the effective dose of PET imaging for female oncology patients using $^{18}$F-FDG. Through radiation decay analysis, we found that the effective dose from PET, using the MIRD phantom as a patient, was determined to be 6.73 mSv. The urinary bladder, brain, and heart were found to have the highest absorbed doses. It is important to note that not all organs absorb the same dose due to variations in constituent materials and organ metabolism. These factors should be taken into consideration to reduce radiation exposure, and mitigate population cancer risk.

**ACKNOWLEDGMENTS**

*Not applicable.*

***Funding:*** Self-funding.

***Conflict of interest:*** The authors declare no conflicts of interest.

***Ethical approval:*** This article does not contain any studies with human participants or animal experiments performed by any of the authors.

[ Downloaded from mail.ijrr.com on 2025-10-14 ]

[ DOI: 10.61186/ijrr.22.3.559 ]

***Author contribution:*** A.O. Ezzati and F. Mohajeri confirmed their contributions in the study's conception and design, as well as the analysis and interpretation of results. F. Mohajeri drafted the manuscript, while the other authors reviewed and revised it M. Studenski assisted with manuscript preparation, editing and interpretation of results. All authors have read and approved the final version of the manuscript.

## REFERENCES


1. Boellaard R, O'Doherty MJ, Weber WA, Mottaghy FM, Lonsdale MN, Stroobants SG, Pruim J, *et al* (2010) FDG PET and PET/CT: EANM procedure guidelines for tumour PET imaging: version 1.0. *European journal of nuclear medicine and molecular imaging,* ***37 (1):*** *181-200.*
2. Said M, Bathumalai J, Kamal I, Razak HA and Karim MA (2020) The Effective Dose Estimation of Patients Administered with 18F-FDG and Ga-68 DOTATATE in PET/CT Examination Associated with Gender and Weight. *Physics and Technology in Medicine,* ***1(1):*** *15-21.*
3. Wang RF, Wang ZG, Yu MM, Chen YH, Shi B and Xue W (2021) 18-F -Fluoroglucosylation of an arginine-arginine-leucine peptide as a potential tumor imaging agent for positron emission tomography. *International Journal of Radiation Research,* ***19(2):*** *357-363. doi:10.52547/ijrr.19.2.14*
4. Gümüş H (2022) Positron CSDA range and stopping power calculations in some human body tissues by using Lenz Jensen atomic screening function. *Radiation Physics and Chemistry,* ***196:*** *110092.*
5. Eckerman K and Endo A (2008) ICRP Publication 107. Nuclear decay data for dosimetric calculations. *Annals of the ICRP,* ***38(3):*** *7-96.*
6. Buvat I and Lazaro D (2006) Monte Carlo simulations in emission tomography and GATE: An overview. *Nuclear Instruments and Methods in Physics Research Section A: Accelerators, Spectrometers, Detectors and Associated Equipment,* ***569(2):*** *323-329.*
7. El-din ME, Mahmoud R, Eid I, El-din ME and Rizk R (2018) Radiation dose rate assessment around patients in PET/CT units. *International Journal of Nuclear Energy Science and Technology,* ***12(1):*** *32-44.*
8. Sarrut D, Bardiès M, Boussion N, Freud N, Jan S, Létang JM, *et al*.Mauxion T (2014) A review of the use and potential of the GATE Monte Carlo simulation code for radiation therapy and dosimetry applications. *Medical physics,* ***41(6Part1):*** *064301.*
9. Sarrut D, Bała M, Bardiès M, Bert J, Chauvin M, Chatzipapas K, Jan S, *et al* (2021) Advanced Monte Carlo simulations of emission tomography imaging systems with GATE. *Physics in Medicine & Biology,* ***66(10):*** *10TR03.*
10. Pérez P and Valente M (2019) DOSIS: An integrated computational tool for patient-specific dosimetry in nuclear medicine by Monte Carlo and dose point kernel approaches. *Applied Radiation and Isotopes,* ***150:*** *135-140.*
11. Valk PE, Abella-Columna E, Haseman MK, Pounds TR, Tesar RD, Myers RW Hofer GA, *et al* (1999) Whole-body PET imaging with [18F] fluorodeoxyglucose in management of recurrent colorectal cancer. *Archives of Surgery,* ***134(5):*** *503-511.*
12. Han EY, Bolch WE and Eckerman KF (2006) Revisions to the ORNL series of adult and pediatric computational phantoms for use with the MIRD schema. *Health Physics,* ***90(4):*** *337-356.*
13. Pelowitz DB (2005) MCNPXTM user's manual. *Los Alamos National Laboratory, Los Alamos*.
14. Boellaard R, Delgado-Bolton R, Oyen WJ, Giammarile F, Tatsch K, Eschner W, Weber WA, *et al* (2015) FDG PET/CT: EANM procedure guidelines for tumour imaging: version 2.0. *European journal of nuclear medicine and molecular imaging,* ***42(2):*** *328-354.*
15. Tarkin JM, Joshi FR, Evans NR, Chowdhury MM, Figg NL, Shah AV, Yu E, *et al* (2017) Detection of atherosclerotic inflammation by 68Ga-DOTATATE PET compared to [18F] FDG PET imaging. *Journal of the American College of Cardiology,* ***69(14):*** *1774-1791.*
16. Mattsson S, Johansson L, Leide Svegborn S, Liniecki J, Noßke D, Riklund K, Carlsson S, *et al* (2015) ICRP publication 128: radiation dose to patients from radiopharmaceuticals: a compendium of current information related to frequently used substances. *Annals of the ICRP, 44*(*2_suppl), 7-321.*
17. Quinn B, Holahan B, Aime J, Humm J, Germain JS and Dauer LT (2012) Measured dose rate constant from oncology patients administered 18F for positron emission tomography. *Medical physics,* ***39(10):*** *6071-6079.*
18. Mattsson S, Johansson L, Svegborn SL, Liniecki J, Noßke D, Riklund K, Carlsson S, *et al* (2015) ICRP Publication 128: Radiation dose to patients from radiopharmaceuticals: a compendium of current information related to frequently used substances. *Ann ICRP, 44*(2 Suppl), *7-321.*
19. Weber W, Czernin J, Anderson C, Badawi R, Barthel H, Bengel F, Graham M, *et al* (2020) The future of nuclear medicine, molecular imaging, and theranostics. *Journal of Nuclear Medicine,* ***61*** *(Supplement 2), 263S-272S.*
20. Wahl RL, Dilsizian V and Palestro CJ (2021) At last, 18F-FDG for Inflammation and Infection! *Journal of Nuclear Medicine,* ***62(8):*** *1048-1049.*
21. Alçin G, Arslan E, Aksoy T, Akbas S and Cermik TF (2022) FDG uptake in breast cancer and Quantitative Assessment of Breast Parenchymal Uptake on 18F-FDG PET/CT: Association with Histopathological, Hormonal status, and Clinical Features. *International Journal of Radiation Research,* ***20(4):*** *815-821. doi:10.52547/ijrr.20.4.13*
22. Demir F and Yanarateş A (2020) Prognostic value of various metabolic parameters on pre-treatment 18-F-FDG PET/CT in patients with stage I-III non-small cell lung cancer. *International Journal of Radiation Research,* ***18(4):*** *799-807. doi:10.52547/ijrr.18.4.799*
23. Khamwan K, Krisanachinda A and Pasawang P (2010) The determination of patient dose from 18F-FDG PET/CT examination. *Radiation protection dosimetry,* ***141(1):*** *50-55.*
24. Karim MKA, Sabarudin A, Muhammad N and Ng KH (2019) A comparative study of radiation doses between phantom and patients via CT angiography of the intra-/extra-cranial, pulmonary, and abdominal/pelvic arteries. *Radiological physics and technology,* ***12 (4):*** *374-381.*
25. Kaushik A, Jaimini A, Tripathi M, D'Souza M, Sharma R, Mishra AK, Dwarakanath BS, *et al* (2013) Estimation of patient dose in 18 F-FDG and 18 F-FDOPA PET/CT examinations. *Journal of cancer research and therapeutics,* ***9(3):*** *477.*
26. Huang B, Law MWM and Khong PL (2009) Whole-body PET/CT scanning: estimation of radiation dose and cancer risk. *Radiology,* ***251(1):*** *166-174.*
27. Andersson M, Johansson L, Minarik D, Mattsson S and Leide-Svegborn S (2014) An internal radiation dosimetry computer program, IDAC 2.0, for estimation of patient doses from radiopharmaceuticals. *Radiation protection dosimetry,* ***162(3):*** *299-305.*
28. Andersson M, Johansson L, Eckerman K and Mattsson S (2017) IDAC-Dose 2.1, an internal dosimetry program for diagnostic nuclear medicine based on the ICRP adult reference voxel phantoms. *EJNMMI research,* ***7(1):*** *1-10.*


[ Downloaded from mail.ijrr.com on 2025-10-14 ]

[ DOI: 10.61186/ijrr.22.3.559 ]